CHINESE OPTICS LETTERS

Vol. 19, No. 5 | May 2021

Engineering the spectral profile of photon pairs by using multi-stage nonlinear interferometers

Mingyi Ma (马明毅)†, Liang Cui (崔 亮)†, and Xiaoying Li (李小英)*

College of Precision Instrument and Opto-Electronics Engineering, Key Laboratory of Opto-Electronics Information Technology, Ministry of Education, Tianjin University, Tianjin 300072, China

*Corresponding author: xiaoyingli@tju.edu.cn

Received August 7, 2020 | Accepted November 20, 2020 | Posted Online March 9, 2021

Using the quantum interference of photon pairs in *N*-stage nonlinear interferometers (NLIs), the contour of the joint spectral function can be modified into an islands pattern. We perform two series of experiments. One is that all of the nonlinear fibers in pulse pumped NLIs are identical; the other is that the lengths of *N* pieces of nonlinear fibers are different. We not only demonstrate how the pattern of spectral function changes with the stage number *N*, but also characterize how the relative intensity of island peaks varies with *N*. The results well agree with theoretical predictions, revealing that the NLI with lengths of *N* pieces of nonlinear fibers following binomial distribution can provide a better active filtering function. Our investigation shows that the active filtering effect of multi-stage NLI is a useful tool for efficiently engineering the factorable two-photon state—a desirable resource for quantum information processing.

Keywords: quantum state engineering; optical parametric amplifier; nonlinear quantum interference.
DOI: 10.3788/COL202119.052702

1. Introduction

The mode structure of quantum optical fields is of utmost importance in quantum information processing (QIP)[1]. The reasons are two-fold. First, many protocols in QIP, such as quantum teleportation and quantum computing, are based on quantum interference, and it is crucial to have mode matching between interfering fields achieve high visibility[2–4]. Second, the mode profile increases the degrees of freedom for quantum fields, which brings the ability to achieve multi-dimensional quantum entanglement and increase the capacity of QIP[1,5]. Therefore, many exquisite efforts have been put on engineering the mode structure of quantum states[2,3,6–15].

Engineering the mode structure of quantum states by using nonlinear interferometers (NLIs) has recently attracted a lot of attention[16–24]. The NLI, which is analogous to a conventional Mach–Zehnder interferometer but with the two beam splitters being substituted by two parametric amplifiers (PAs), was originally proposed to achieve the Heisenberg limit in precision phase measurement[25] and had been used to demonstrate interesting applications in quantum metrology, spectroscopy, optical imaging, etc.[26–29]. When the NLI is used to modify the spectral property of photon pairs, the phase matching of PAs is controlled by the nonlinear medium, while spectral shaping is obtained through dispersion control of the interferometer. The separation of the mode control from nonlinear interaction brings the advantages in engineering photon pairs[16] that simultaneously possess the features of high purity, high collection efficiency, high brightness, and high flexibility in wavelength and bandwidth selection, and these advantages had been verified by the proof of principle experiments realized by pulse pumped two- and three-stage NLIs[21–23].

The theoretical analysis shows that finer mode control can be realized if the stage number of NLI, N (the number of PAs or nonlinear media), is greater than two[16]. For the joint spectral function (JSF) of signal and idler photon pairs with island patterns tailored by the active filtering effect of NLI, the separation between two adjacent islands increases with N. When the gain of each PA is the same, the interference factor of the JSF, $\frac{\sin N\theta}{\sin \theta}$ (with θ denoting the phase shift induced by dispersion control in NLI), is similar to that of a multi-slit interferometer in classical optics. In this case, there are mini-maxima existing in between the main maxima, leading to non-ideal isolation between two adjacent islands. For the frequency uncorrelated photon pairs extracted from one island, the non-ideal isolation results in reduced collection efficiency[21–23]. When the gains of PAs are changed by properly arranging the lengths of nonlinear media, the influence of the mini-maxima on the isolation between adjacent islands can then be eliminated. However, most of the NLI experiments presented so far[21–24,26–29] consist of nonlinear media with identical lengths. Modifying the JSF by using multi-stage NLI with uneven length nonlinear media has not been experimentally demonstrated yet.

© 2021 Chinese Optics Letters

In this paper, we experimentally investigate the JSF of photon pairs generated from four wave mixing (FWM) in pulse pumped multi-stage NLIs, which are formed by a sequential array of nonlinear fibers, with a gap in between made of a linear dispersive medium of standard single mode fibers (SMFs). To illustrate that the multi-stage NLIs consisting of nonlinear fibers with uneven length have advantages in providing a better active filtering function for reshaping the JSF, we perform two series of experiments and compare their results. One is where all of the nonlinear fibers in NLI with $N = 2, 3, 4$ are identical; the other is when the lengths of N ($N > 2$) pieces of nonlinear fibers follow binomial distribution.

2. Experiments and Results

Our experimental setup is shown in Fig. 1. The NLI is formed by N pieces of dispersion shifted fibers (DSFs) with $N-1$ pieces of standard SMFs in between. The DSF functions as a nonlinear medium of FWM; the SMF functions as a linear dispersion medium and is used to introduce phase shift in NLI. Since the spatial mode of the optical fields involved in FWM is well confined by the waveguide structure of optical fibers, we can focus on studying the temporal or spectral mode structure of photon pairs. For each DSF, the zero dispersion wavelength is $\lambda_0 = 1552.5$ nm, the dispersion slope at λ_0 is $D_{\text{slope}} = 0.075\ \text{ps}/(\text{km}\cdot\text{nm}^2)$, and the nonlinear coefficient γ is $2\ (\text{W}\cdot\text{km})^{-1}$. When the NLI is pumped with a train of laser pulses with a central wavelength of $\lambda_{p0} = 1553.3$ nm, the phase matching condition of FWM, $\Delta k = \frac{\lambda_{p0}^2}{8\pi c} D_{\text{slope}}(\lambda_{p0} - \lambda_0)(\omega_s - \omega_i)^2 - 2\gamma P_p \approx 0$, is satisfied[23], where c is the speed of light in vacuum, and P_p is the peak pump power. In the spontaneous FWM process, two pump photons at frequency ω_p scatter through the $\chi^{(3)}$ Kerr nonlinearity of DSF to create a pair of quantum correlated signal and idler photons at frequencies of ω_s and ω_i, respectively. The dispersion coefficient of the standard SMF in the 1550 nm band is about $D_{\text{SMF}} = 17\ \text{ps}/(\text{nm}\cdot\text{km})$, so the phase matching condition of FWM is not satisfied in the SMF. The spectral shaping of photon pairs is obtained through the control of linear dispersion media of SMFs in the NLI.

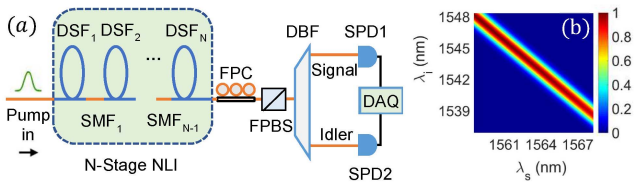

Fig. 1. (a) Experimental setup of generating photon pairs from an N-stage nonlinear interferometer (NLI) consisting of N pieces of nonlinear media of dispersion shifted fibers (DSFs) and $N-1$ pieces of phase shifters of standard single mode fibers (SMFs). DBF, dual-band filter; FPC, fiber polarization controller; FPBS, fiber polarization beam splitter; SPD, single photon detector; DAQ, data acquisition system. (b) The contour of JSI $|F(\omega_s,\omega_i)|^2$ for photon pairs generated from a single piece of DSF.

The pump of the NLI is obtained by passing the output of a femtosecond fiber laser through a bandpass filter (see Ref. [21] for details). The full width at half-maximum (FWHM) and repetition rate of transform limited pump pulses are 1.4 nm and 36.8 MHz, respectively. In the NLI, the transmission losses of DSFs and SMFs, which are about 0.3 dB/km and 0.2 dB/km, respectively, are negligible, and the loss induced by each splicing point between the DSF and SMF is less than 4%. In the experiments presented hereinafter, the length of each SMF, L_{DM}, is fixed at 10 m, while the number and length of DSFs can be varied.

Since the internal loss of our NLI is negligibly small, when the pump power is low and the length of each DSF is identical, the JSF of photon pairs at the output of NLI can be approximately expressed as[16]

$$F_{\text{NLI}}^{\text{S}}(\omega_s,\omega_i) = F(\omega_s,\omega_i) \times H(\theta) = g\ \exp\left[-\frac{(\omega_s+\omega_i-2\omega_{p0})^2}{4\sigma_p^2}\right] \times \text{sinc}\left(\frac{\Delta kL}{2}\right) \times H(\theta), \tag{1}$$

where $F(\omega_s,\omega_i) = g\ \exp\left[-\frac{(\omega_s+\omega_i-2\omega_{p0})^2}{4\sigma_p^2}\right]\text{sinc}(\frac{\Delta kL}{2})$ with gain coefficient $g \propto \gamma P_p L \ll 1$ is the JSF of photon pairs generated by a single piece DSF, the superscript "S" denotes that the length of each DSF in the NLI is the same, and $\omega_{p0} = 2\pi c/\lambda_{p0}$ and σ_p are the central frequency and bandwidth of the pump. In Eq. (1),

$$H(\theta) = e^{i(N-1)\theta}\frac{\sin N\theta}{\sin\theta} \tag{2}$$

is the interference factor of the NLI, where $\theta = (\Delta kL + \Delta\phi_{\text{DM}})/2$ with $\Delta\phi_{\text{DM}}$ representing the phase shift induced by the SMF as the overall phase difference between pump and photon pairs of adjacent DSFs. In our experiment, the approximations $\Delta kL \to 0$ and $\text{sinc}(\frac{\Delta kL}{2}) \to 1$ hold due to the satisfaction of the phase matching condition in the DSF. For the SMF with $L_{\text{DM}} = 10$ m, the amount of phase shift $\Delta\phi_{\text{DM}}$ is much greater than that of the term ΔkL, and we have the approximation[21,23]

$$\theta \approx \frac{\Delta\phi_{\text{DM}}}{2} = \frac{\lambda_{p0}^2 D_{\text{SMF}} L_{\text{DM}}(\omega_s-\omega_i)^2}{16\pi c}. \tag{3}$$

When the linear dispersion media of SMFs still have the same length but the lengths of DSFs are arranged by using binomial distribution[16],

$$L_n = L_1 C_{N-1}^{n-1} = L_1\frac{(N-1)!}{(n-1)!(N-n)!}, \tag{4}$$

and the JSF of photon pairs can then be approximately expressed as[16]

$$F_{\mathrm{NLI}}^{(\mathrm{UN})}(\omega_s,\omega_i) \approx \exp\left[-\frac{(\omega_s+\omega_i-2\omega_{p0})^2}{4\sigma_p^2}\right] \times K(\theta), \quad (5)$$

with the interference factor given by

$$K(\theta) = \sum_{n=1}^{N} L_n e^{2i(n-1)\theta} = L_1(1+e^{2i\theta})^{N-1}, \quad (6)$$

where L_n is the length of DSF_n ($n = 1, 2, \ldots, N$) in the NLI [see Fig. 1(a)], the superscript "UN" refers to the NLI with uneven length DSFs, and θ is the same as in Eq. (3). Therefore, if the different sections of nonlinear media in the NLI follow a binomial pattern, e.g., $L_1 : L_2 : L_3 = 1 : 2 : 1$ for $N = 3$ and $L_1 : L_2 : L_3 : L_4 = 1 : 3 : 3 : 1$ for $N = 4$, there are no mini-maxima in $|K(\theta)|^2$. On the contrary, the H function in Eq. (2) normally gives the $(N-1)$th harmonic of $\cos 2\theta$, i.e., $\cos 2(N-1)\theta$.

To experimentally characterize the spectral profile of photon pairs, we need to extract the signal and idler photon pairs at the output of the NLI. A fiber polarization controller (FPC) placed in front of the fiber polarization beam splitter (FPBS) is used to select the signal and idler photon pairs co-polarized with the pump and to reject the Raman scattering (RS) cross polarized with the pump[30]. Because the conversion efficiency of FWM in the NLI is relatively low, about 0.01 photon pair is produced in a 100-m-long DSF when the number of pump photons contained in a pulse of 4 ps duration is about 10^7. Thus, to reliably detect the correlated photon pairs by single photon detectors (SPDs), a pump to photon pair rejection ratio in excess of 110 dB is required. We achieve this by passing the output of the NLI through a dual-band filter (DBF), which is realized by cascading a notch filter with a programmable optical filter (POF, model: Finisar Wave shaper 4000S). For each pass band of the DBF, the spectrum is rectangularly shaped, and both the central wavelength and bandwidth are tunable.

Two superconducting nanowire SPDs, SPD1 and SPD2, followed by a data acquisition system (DAQ), are utilized to count the signal and idler photons. The detection efficiencies in both signal and idler bands are about 10% when the efficiencies of the SPDs (~80%) and transmission efficiency of the DBF are included.

We first measure the JSF of photon pairs generated from NLI when the DSFs are the same and the stage number is $N = 2, 3, 4$, respectively. In the experiment, the length of each DSF is 100 m, the average pump power is fixed at 60 μW, and the bandwidth for both the signal and idler pass bands of the DBF is set to ~0.16 nm (0.02 THz in frequency). During measurement, the central wavelength of the DBF in the signal (idler) channel is scanned from 1558.5 nm (1548.4 nm) to 1568.3 nm (1537.9 nm) with a step of ~0.16 nm (0.02 THz in frequency). Under each wavelength setting of the DBF, we not only record the single counts of individual SPD1 and SPD2, respectively, but also measure the two-fold coincidence counts of two SPDs, respectively, for the signal and idler photons originating from the same pump pulse and adjacent pulses, C_c and C_{acc}. We then deduce the true coincidence counts of photon pairs C_T by subtracting the measured C_{acc} from C_c. Figure 2(c) plots the contour maps of true coincidences in the wavelength coordinates of λ_s and λ_i, which reflects the joint spectral intensity (JSI) $|F_{\mathrm{NLI}}^{\mathrm{S}}(\omega_s,\omega_i)|^2$ of photon pairs[31,32]. Clearly, the contour maps of true coincidence for the cases of $N = 2, 3, 4$ in Fig. 2(c) exhibit island patterns, which are obviously different from the JSI of photon pairs produced by a single piece of DSF [see Fig. 1(b)]. For each plot in Fig. 2(c), the distance between the maxima of adjacent primary islands decreases with the increase of detuning $(\lambda_s - \lambda_i)$ because the phase shift θ in Eq. (3) quadratically depends on the detuning of photon pairs. For the convenience of recognition, we label the primary islands with $m = 1, 2, 3, 4$, and the order number m increases with the detuning $(\lambda_s - \lambda_i)$. From Fig. 2(c), one sees that the variation trend for patterns of JSF has the following distinct features. First, the central wavelengths of the primary islands do not vary with N. In each plot of Fig. 2(c), the central wavelengths of the islands labelled $m = 1, 2, 3, 4$ in the signal (idler) band are centered at about 1560.4 nm (1546.3 nm), 1563.3 nm (1543.5 nm), 1565.5 nm (1541.3 nm), and 1567.4 nm (1539.5 nm), respectively. Second, for the island with a fixed-order number m, the width of the island decreases with the increase of N. Accordingly, the separation between adjacent islands increases with N. Third, the peak intensity for the measured true coincidences of the NLI

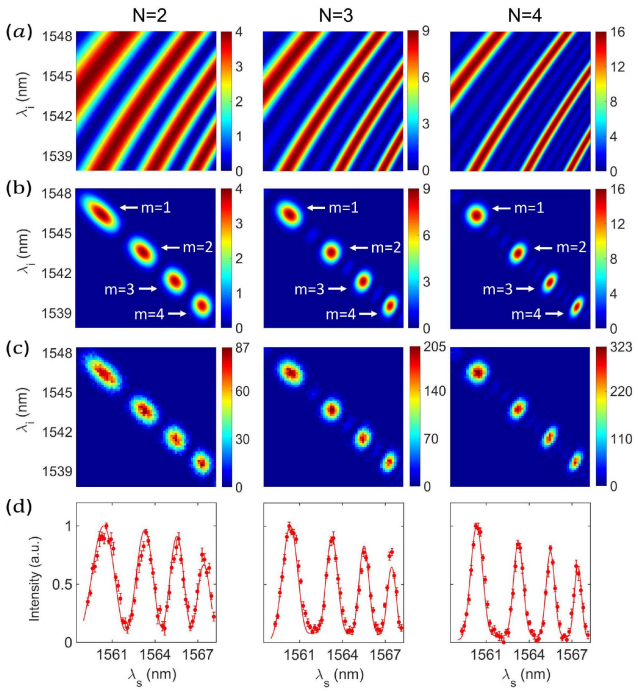

Fig. 2. Results for N-stage NLI with N = 2, 3, 4 when the lengths of each DSF and SMF in the NLI are 100 m and 10 m, respectively. (a), (b) The contours of interference factor $|H(\theta)|^2$ and JSI $|F_{\mathrm{NLI}}^{\mathrm{S}}(\omega_s,\omega_i)|^2$ calculated by substituting experimental parameters into Eqs. (2) and (1), respectively. (c) Contour maps of measured true coincidence of photon pairs, which reflect the JSI of photon pairs. (d) Measured (dots) and calculated (solid curves) marginal intensity distributions of signal photons.

increases with N. The counting rates corresponding to the highest peaks of the primary islands are 87 ± 5, 205 ± 10, and 323 ± 18 counts/s for $N = 2, 3, 4$, respectively. The results show that the peak of the island increases with the scale of N^2, as predicted by Eq. (2). Fourth, $N - 2$ secondary islands exist between two adjacent primary islands. The counting rates for all of the peaks of the secondary islands are around 20–30 counts/s. So, the ratio between the intensities of the primary and secondary islands increases with the increase of N. As a result, the influence of secondary islands upon the isolation between two primary islands will decrease for N with a larger number [17].

To compare the measured JSIs with theoretical predictions, we calculate the contours of JSI for the case of $N = 2, 3, 4$ by substituting the experimental parameters of our NLI into Eqs. (1)–(3), as shown in Fig. 2(b). To better illustrate how the quantum interference of photon pairs in NLI influences the JSF, the contours of interference factor $|H(\theta)|^2$ for $N = 2, 3, 4$ are calculated as well, as shown in Fig. 2(a). One sees that the symmetry lines of $|H(\theta)|^2$ in Fig. 2(a) are perpendicular to that of $|F(\omega_s,\omega_i)|^2$ in Fig. 1(b). As a result, the JSIs of the NLI in Fig. 2(b) exhibit island patterns, and the main maxima occur at $\theta = m\pi$ $(m = 1, 2, \ldots)$. Depending on the stripe width of $|H(\theta)|^2$, $\sigma_{\text{int}}^2 = 4c/[(N-1)m\lambda_{p0}^2 D_{\text{SMF}} L_{\text{DM}}]$, the pattern of the primary island changes with variations of the stage number N, order number of island m, and pump bandwidth[16,23]. With the increase of N and m, the width of the primary island decreases. The comparison of Figs. 2(c) and 2(b) shows that the experimental results agree well with the theoretical predictions.

It's worth noting that the multi-stage NLI with N $(N > 2)$ pieces of identical nonlinear media had already been experimentally realized in a fiber-based NLI and $\chi^{(2)}$ crystal-based NLI[22,23,29], respectively. In particular, in Ref. [29], the JSIs of the NLI were measured when the stage number was $N = 2, 3, 4, 5$, respectively, while other experimental parameters were fixed. Although the results qualitatively agree with theory, there are obvious deviations from theoretical predictions due to the problem of imperfect alignment in bulk-crystal-based systems[29]. Here, we characterize the islands pattern of JSI from top to bottom by using the advantages of the fiber-based NLI: freedom from misalignment and low internal loss for all of the optical fields involved in FWM. In addition to illustrating how the center and width of the islands change with the stage number N and order number m, we reveal how the relative intensity of island peaks varies with N. The latter has not been demonstrated before.

In order to clearly visualize that the NLI functions as an active filter of photon pairs, we deduce the marginal intensity distribution in signal and idler fields from the counting rates of SPD1 and SPD2, respectively. Because the data of the two individual fields is similar, for the sake of brevity, we only show the results in the signal field. Note that for our fiber-based NLI, there is RS accompanying the FWM[30]. The existence of RS does not affect the measured JSI in Fig. 2, because there is no quantum correlation for the RS photons in the signal and idler bands. However, when the active filtering effect of the NLI is characterized by observing the interference in an individual signal (idler) band, which is equivalent to projecting the contour of JSI along the signal (idler) axis, the contribution of RS should be subtracted.

When the pass bands of the DBF are scanned, at each wavelength setting, we measure the counting rates $R_{s(i)}$ in individual signal (idler) channels at different levels of average pump power P_a and then fit the measured data with a second-order polynomial $R_{s(i)} = s_1 P_a + s_2 P_a^2$, where s_1 and s_2 are the fitting parameters. The linear and quadratic terms, $s_1 P_a$ and $s_2 P_a^2$, are, respectively, proportional to the intensities of RS and FWM. Figure 3 shows two typical sets of raw data, which are obtained by setting the wavelength of the DBF in the signal band at 1560.4 nm and 1561.9 nm, respectively. The two wavelengths, respectively, correspond to the peak and valley of the islands with $m = 1$ and $N = 4$ [see Fig. 2(c)]. The fitting results of the data show that the linear parts in both Figs. 3(a) and 3(b) are quite high. This is because our NLI is simply placed at room temperature to avoid unnecessary complexity. Considering the RS can be significantly suppressed by cooling NLI[21,23,33], here we focus on studying the photon pairs via FWM. Compared with the quadratic part (dotted curve) in Fig. 3(a), we find that the value of the quadratic term in Fig. 3(b) is quite small due to the destructive interference effect that occurred at the wavelength of ~1561.9 nm in the NLI with $N = 4$. When pump power is 60 μW, the ratio between the quadratic terms in Figs. 3(a) and 3(b) is about 16.3, indicating that the visibility of the interference fringe individual signal field originating from FWM is around 88%, which is slightly lower than the theoretically calculated result of ~92%. We think the deviation from theoretical prediction is caused by the internal loss in the NLI (~15% for $N = 4$) due to the imperfect splicing.

When the interference fringe in the individual signal (idler) field is used to characterize the active filtering effect of the NLI, we only consider the contribution of photons originating from FWM, which are deduced from the quadratic part of the second-order polynomial fitting function. Figure 2(d) shows the normalized rate of single counts (via FWM) as a function of the wavelength in the signal channel. Each plot in Fig. 2(d) exhibits an interference pattern, illustrating that the NLI

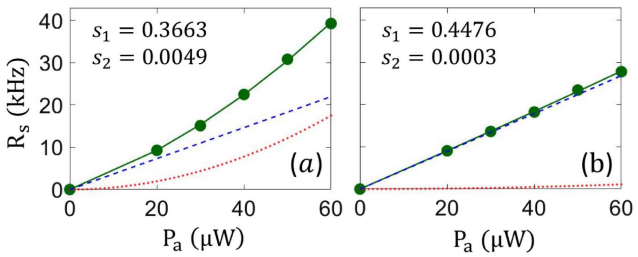

Fig. 3. Measured counting rate (dots) R_s as a function of the average pump power P_a for the photons in an individual signal band centering at (a) 1560.4 nm and (b) 1561.9 nm, respectively. The solid curve $R_s = s_1 P_a + s_2 P_a^2$ is the fitting function of raw data (dots); dashed and dotted lines are the linear term $s_1 P_a$ and quadratic term $s_2 P_a^2$, respectively.

functions as an active filter of photon pairs. The data (dots) in Fig. 2(d) is obtained by subtracting the RS from the directly measured counts of SPD1, as illustrated in Fig. 3. We find that the measured intensity distributions agree with the theoretically calculated results (solid curves). For the interference fringes corresponding to a fixed peak wavelength, which are originated from the islands with the same order number m, the fringe width decreases with the increase of N. The visibility of the interference fringe, defined by $V_m = (I^m_{\max} - I^m_{\min})/(I^m_{\max} + I^m_{\min})$ with $I^m_{\max}$ and $I^m_{\min}$, respectively, denoting the normalized intensity at the peak and trough, increases with N. One sees that V_m is the lowest for the case of $N = 2$ due to the existence of overlap between two adjacent islands. However, even if N is increased to a larger number, the minimum of the normalized intensity (single count rates) $I^m_{\min}$ is still away from zero due to the secondary islands existing in between adjacent primary islands. Note that in the process of selecting the photon pairs with the spectral profile determined by one specific island, the bandwidth of filters used to efficiently select out photon pairs should be properly set. By doing so, one island can be picked out as a whole, and the isolation to adjacent islands is as much as possible[23]. Hence, the collection efficiency of photon pairs, characterized by the probability of detecting the photon at the signal (idler) band for a photon detected in the idler (signal) band, is closely related to interference fringe presented in marginal intensity distribution. To improve the collection efficiency, the visibility of the corresponding fringe in Fig. 2(d) should be as high as possible. The non-ideal visibility (less than one) will prevent the collection efficiency of photon pairs from reaching the ideal value of one, in particular, when the NLI is designed to engineer the factorable state[16,21,23].

To illustrate how to get rid of the mini-maxima in between the main maxima in the JSI in Fig. 2, we then perform the second experiment to verify the spectral profile of uneven N-stage NLI with $N = 3, 4$, respectively. In the experiment, the parameters are the same as that in Fig. 2, except for the lengths of DSFs, which follow binomial distribution [see Eq. (4)]. When $N = 3$, the lengths of three DSFs, L_1, L_2, and L_3, are 50, 100, and 50 m, respectively; when $N = 4$, the lengths of four DSFs, L_1, L_2, L_3, and L_4, are 33.3, 100, 100, and 33.3 m, respectively. Figure 4(c) shows the contour maps of true coincidences in the wavelength coordinates of the signal and idler, λ_s and λ_i. The counting rates corresponding to the highest peaks of the islands are 71 ± 3 and 120 ± 5 counts/s for $N = 3, 4$, respectively. The centers of the islands and the variation tendencies of the islands are the same as those of the $N = 3$ and $N = 4$ cases in Fig. 2. The separation between two adjacent islands still increases with N, but the secondary islands do not exist anymore.

We also calculate the contours of interference factor $|K(\theta)|^2/L_1^2$ and JSI $|F^{(\mathrm{UN})}_{\mathrm{NLI}}(\omega_s,\omega_i)|^2$ of the uneven N-stage NLI by substituting the experimental parameters into Eqs. (5) and (6), as shown in Figs. 4(a) and 4(b). It is clear that the variation tendency of $|K(\theta)|^2/L_1^2$ is similar to that in Fig. 2(a), except that the mini-maxima do not exist anymore. The stripe width of the main maxima of $|K(\theta)|^2/L_1^2$ still narrows as N increases, leading

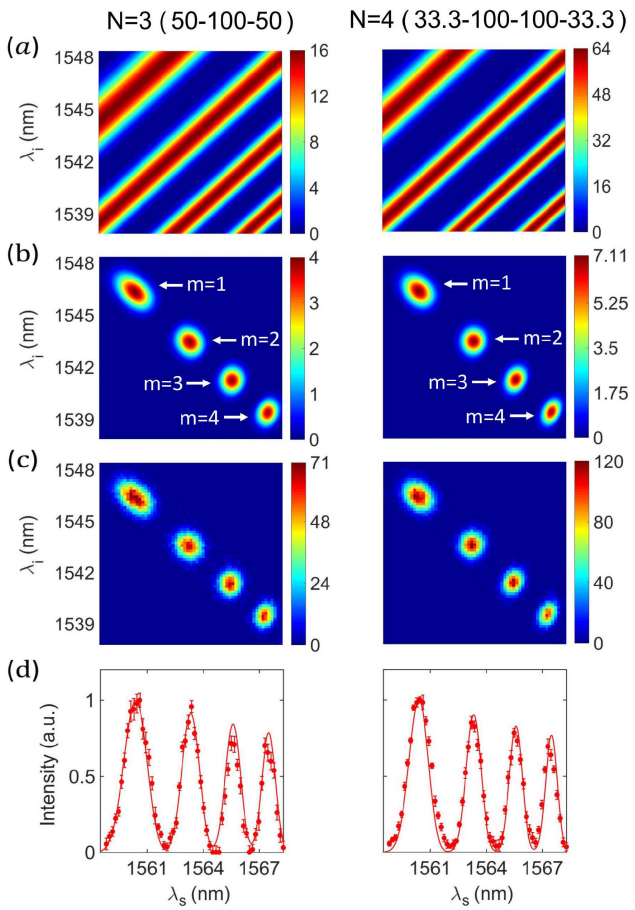

Fig. 4. Results for uneven N-stage NLI, in which the lengths of DSFs, labelled in the top for different stage number N, follow binomial distribution. (a), (b) The calculated contours of interference factor $|K(\theta)|^2/L_1^2$ and JSI $|F^{(\mathrm{UN})}_{\mathrm{NLI}}(\omega_s,\omega_i)|^2$ [see Eqs. (5) and (6)], respectively. (c) Contour maps of true coincidence of photon pairs, reflecting the JSI of photon pairs. (d) Measured (dots) and calculated (solid curves) marginal intensity distributions of signal photons.

to enlarged island separation in the JSF. Comparing Fig. 4(c) with Fig. 4(b), we find the measured islands pattern of the JSI agrees well with the theoretical prediction.

Additionally, we characterize the active filter function of the uneven N-stage NLI by deducing the marginal intensity distribution in individual signal and idler fields. The procedure of processing data is similar to that in Figs. 2(d) and 3. Figure 4(d) shows the data (dots) in the signal channel. We find that the data agrees with the theoretically calculated results (solid curves). Compared with Fig. 2(d), one sees that, for the NLI with same stage number of N, the visibility of interference fringes in Fig. 4(d) is slightly higher.

It is well known that the spectrally factorable photon pairs with high collection efficiency are the desirable resources of QIP. Recent investigation shows that the quantum interference in NLI provides an alternative approach for achieving this kind of photon pairs[16,23,24]. So, we pay more attention to the round shaped islands, from which the spectrally factorable state can be

obtained without sacrificing collection efficiency. For the round islands in Fig. 2, obtained under the condition of (i) $N = 2$, $m = 4$, (ii) $N = 3$, $m = 2$, and (iii) $N = 4$, $m = 1$, the visibility in Fig. 2(d) obviously deviates from the ideal results of one due to the existence of overlap ($N = 2$) or the mini-maxima ($N \geq 3$). While for both the cases of (ii) $N = 3$, $m = 2$ and (iii) $N = 4$, $m = 1$ in Fig. 4, the fringe visibilities of the round island in Fig. 4(d) are approaching the ideal value of one because of the increased separation and the elimination of mini-maxima. This analysis and comparison indicate that if the NLI is used to engineer a factorable state, a higher collection efficiency of photon pairs can be obtained by the properly designed uneven N-stage NLI with $N \geq 3$.

3. Summary and Discussion

In conclusion, we have experimentally investigated the spectral profile of photon pairs generated from pulse pumped multi-stage NLIs, in which DSFs and standard SMFs, respectively, function as nonlinear fibers and linear dispersion media. Since the fiber-based NLI has the advantages of freedom from misalignment and low internal loss, we are able to comprehensively characterize the JSF of photon pairs. The experimental results agree with theoretical predictions. Our investigation shows that although the photon pairs produced by a single piece DSF via FWM are frequency anti-correlated, their mode profile can be flexibility modified by the active filtering effect that originated from the quantum interference in the N-stage NLI, and the NLI with stage number $N > 2$ has more flexibility in modifying the mode structure of photon pairs.

Moreover, the experimental results reveal that the uneven multi-stage NLI can provide a better active filtering function: the separation between adjacent islands in the contour of the JSF increases with N, and there are no mini-maxima between two primary maxima. To the best of our knowledge, this is the first experimental demonstration using an uneven multi-stage NLI to modify JSF. In principle, the perfect active filtering effect is achievable by increasing N to a large number, even if each nonlinear medium in the NLI is identical[17]. However, in practice, the increased stage number usually accompanies increased internal loss of NLI, which will not influence the islands pattern of JSF for the fiber-based NLI but introduce uncorrelated background noise photons in individual signal and idler bands. Therefore, the feature of the uneven multi-stage NLI is useful for efficiently engineering the factorable two-photon state, in particular, when the stage number of the NLI is not large.

Acknowledgement

This work was supported by the National Key Research and Development Program of China (No. 2016YFA0301403), the National Natural Science Foundation of China (Nos. 11527808 and 11874279), and the Science and Technology Program of Tianjin (No. 18ZXZNGX00210).

†These authors contributed equally to this work.

References

1. C. Fabre and N. Treps, "Modes and states in quantum optics," Rev. Mod. Phys **92**, 035005 (2020).
2. J. Pan, D. Bouwmeester, W. Harald, and Z. Anton, "Experimental entanglement swapping: entangling photons that never interacted," Phys. Rev. Lett. **80**, 3891 (1998).
3. D. Bouwmeester, J. Pan, M. Klaus, E. Manfred, W. Harald, and Z. Anton, "Experimental quantum teleportation," Nature **390**, 575 (1997).
4. E. Knill, R. Laflamme, and G. J. Milburn, "A scheme for efficient quantum computation with linear optics," Nature **409**, 46 (2001).
5. B. Brecht, D. V. Reddy, C. Silberhorn, and M. G. Raymer, "Photon temporal modes: a complete framework for quantum information science," Phys. Rev. X **5**, 041017 (2015).
6. Z. Y. Ou, "Parametric down-conversion with coherent pulse pumping and quantum interference between independent fields," Quantum Semiclass. Opt. **9**, 599 (1997).
7. W. P. Grice and I. A. Walmsley, "Spectral information and distinguishability in type-II down-conversion with a broadband pump," Phys. Rev. A **56**, 1627 (1997).
8. P. J. Mosley, J. S. Lundeen, B. J. Smith, P. Wasylczyk, A. B. U'Ren, C. Silberhorn, and I. A. Walmsley, "Heralded generation of ultrafast single photons in pure quantum states," Phys. Rev. Lett. **100**, 133601 (2008).
9. K. Garay-Palmett, H. J. McGuinness, O. Cohen, J. S. Lundeen, R. Rangel-Rojo, A. B. U'Ren, M. G. Raymer, C. J. McKinstrie, S. Radic, and I. A. Walmsley, "Photon pair-state preparation with tailored spectral properties by spontaneous four-wave mixing in photonic-crystal fiber," Opt. Express **15**, 14870 (2007).
10. O. Cohen, J. S. Lundeen, B. J. Smith, G. Puentes, P. J. Mosley, and I. A. Walmsley, "Generation of uncorrelated photon-pairs in an optical fiber," Phys. Rev. Lett. **102**, 123603 (2009).
11. L. Cui, X. Li, and N. Zhao, "Minimizing the frequency correlation of photon pairs in photonic crystal fibers," New. J. Phys. **14**, 123001 (2012).
12. P. G. Evans, R. S. Bennink, W. P. Grice, T. S. Humble, and J. Schaake, "Bright source of spectrally uncorrelated polarization-entangled photons with nearly single-mode emission," Phys. Rev. Lett. **105**, 253601 (2010).
13. A. M. Brańczyk, A. Fedrizzi, T. M. Stace, T. C. Ralph, and A. G. White, "Engineered optical nonlinearity for quantum light sources," Opt. Express **19**, 55 (2011).
14. J. Su, L. Cui, Y. Li, and X. Li, "Micro/nano-fiber-based source of heralded single photons at the telecom band," Chin. Opt. Lett. **16**, 041903 (2018).
15. M. Hu, Y. Chen, G. Li, and X. Chen, "Multichannel polarization-entangled photon-pair source for entanglement distribution," Chin. Opt. Lett. **14**, 061301 (2016).
16. L. Cui, J. Su, J. Li, Y. Liu, X. Li, and Z. Y. Ou, "Quantum state engineering by nonlinear quantum interference," Phys. Rev. A **102**, 033718 (2020).
17. A. B. U'Ren, C. Silberhorn, K. Banaszek, I. A. Walmsley, R. Erdmann, W. P. Grice, and M. G. Raymer, "Generation of pure-state single-photon wave packets by conditional preparation based on spontaneous parametiric down conversion," Laser Phys. **15**, 146 (2005).
18. G. Frascella, E. E. Mikhailov, N. Takanashi, R. V. Zakharov, O. V. Tikhonova, and M. V. Chekhova, "Wide-field SU(1,1) interferometer," Optica **6**, 1233 (2019).
19. G. Frascella, R. V. Zakharov, O. V. Tikhonova, and M. V. Chekhova, "Experimental reconstruction of spatial Schmidt modes for a wide-field SU(1,1) interferometer," Laser Phys. **29**, 124013 (2019).
20. S. Lemieux, M. Manceau, P. R. Sharapova, O. V. Tikhonova, R. W. Boyd, G. Leuchs, and M. V. Chekhova, "Engineering the frequency spectrum of bright squeezed vacuum via group velocity dispersion in an SU(1,1) interferometer," Phys. Rev. Lett. **117**, 183601 (2016).
21. J. Su, L. Cui, J. Li, Y. Liu, X. Li, and Z. Y. Ou, "Versatile and precise quantum state engineering by using nonlinear interferometers," Opt. Express **27**, 20479 (2019).
22. J. Li, J. Su, L. Cui, X. Li, and Z. Y. Ou, "High visibility Hong–Ou–Mandel interference between independent single photon sources obtained from multistage nonlinear interferometers," in *Conference on Lasers and Electro-Optics* (2019), paper FTh3D.5.
23. J. Li, J. Su, L. Cui, T. Xie, Z. Y. Ou, and X. Li, "Generation of pure-state single photons with high heralding efficiency by using a three-stage nonlinear interferometer," Appl. Phys. Lett. **116**, 204002 (2020).

24. N. Huo, Y. Liu, J. Li, L. Cui, X. Chen, R. Palivela, T. Xie, X. Li, and Z. Y. Ou, "Direct temporal mode measurement for the characterization of temporally multiplexed high dimensional quantum entanglement in continuous variables," Phys. Rev. Lett. **124**, 213603 (2020).
25. B. Yurke, S. L. McCall, and J. R. Klauder, "SU(2) and SU(1,1) interferometers," Phys. Rev. A **33**, 4033 (1986).
26. M. V. Chekhova and Z. Y. Ou, "Nonlinear interferometers in quantum optics," Adv. Opt. Photon. **8**, 104 (2016).
27. Z. Y. Ou and X. Li, "Quantum entangled interferometers," APL Photon. **5**, 080902 (2020).
28. D. A. Kalashnikov, A. V. Paterova, S. P. Kulik, and L. A. Krivitsky, "Infrared spectroscopy with visible light," Nat. Photon. **10**, 98 (2016).
29. A. V. Paterova and L. A. Krivitsky, "Nonlinear interference in crystal superlattices," Light Sci. Appl. **9**, 82 (2020).
30. X. Li, J. Chen, P. Voss, J. E. Sharping, and P. Kumar, "All-fiber photon-pair source for quantum communications: improved generation of correlated photons," Opt. Express **12**, 3737 (2004).
31. Y.-H. Kim and W. P. Grice, "Measurement of the spectral properties of the two-photon state generated via type II spontaneous parametric downconversion," Opt. Lett. **30**, 908 (2005).
32. M. Liscidini and J. E. Sipe, "Stimulated emission tomography," Phys. Rev. Lett. **111**, 193602 (2013).
33. S. D. Dyer, B. Baek, and S. W. Nam, "High-brightness, low-noise, all-fiber photon pair source," Opt. Express **17**, 10290 (2009).